Jurnal Teknologi

Full paper

Structural Analysis of UTM Single-Seat Helicopter Chassis

Mohd Shariff bin Ammoo*, Ziad Bin Abdul Awal, Khairul Shamil bin Khairudin

Faculty of Mechanical Engineering, Universiti Teknologi Malaysia, 81310 UTM Johor Bahru, Johor Malaysia

**Corresponding author: mshariff@fkm.utm.my*

Article history

Received 1 Oct 2013
Received in revised form 1 Sep 2014
Accepted 4 Sep 2014

Graphical abstract

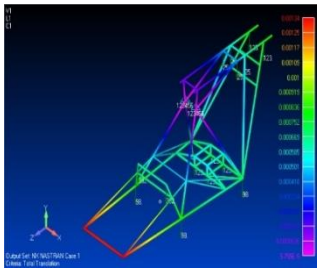

Deformation on the helicopter chassis

Abstract

Structural strength is just as important as any other measures for a performance vehicle - let it be in air, land or water. Chassis is the most critical constituent in keeping the integrity of a vehicular structure. Likewise, helicopter chassis is like its skeleton. Devoid of it, the helicopter will neither take shape nor conserve the structural strength necessary. This research took the liberty of appraising the structural stiffness of the chassis for UTM Single-Seat Helicopter which is being developed at Universiti Teknologi Malaysia (UTM). This helicopter uses space frames as the main chassis structure. The material used for this chassis is AISI 4130 steel. Static analysis of the chassis was conducted specifically during hovering condition. The analysis started with modelling and simulating the chassis using Finite Element Analysis (FEA) software. Data obtained through FEA simulation were then tested and verified using the experimental data. The results obtained were intriguing and in line with the FAA standard Regulation.

Keywords: Chassis; stiffness; deformation; combined stress; finite element analysis (fea)

1.0 INTRODUCTION

The aviation industry has flourished with ground-breaking designs, far-reaching notions and audacious materials since the trailblazing breakthrough by the Wright brothers [1]. Materials and nimble design plays a pivotal role in the present aviation industry [2]. Though the aerodynamics of the helicopter rotor is deliberated as one of the most enlivening and distressing deterrent encountered by the aerodynamicists around the world, structural veracity is a prodigious apprehension as well [1, 3]. Indisputably, structural strength transpires to be an imperative element in aircraft design [4]. One of the most substantial part of any vehicular structure is the chassis. Chassis is the central frame of a vehicle that fascinate different loads and integrate other parts and components of the vehicle together [5-6]. For a helicopter, chassis is the main structure of the fuselage section. It abets in absorbing the loads generated during the phase of lifting, thrusting as well as landing [7]. Chassis can be considered as one of the key elements of a helicopter as it plays a major part in ensuring safety, performance, and airworthiness during operation [8]. Therefore, meticulous study is required on the chassis in order to ensure the performance and integrity of the structure in real operational conditions. Bearing this in mind, this research took the liberty of conducting conscientious structural analysis of UTM Single-Seat Helicopter chassis. UTM Single-Seat Helicopter is a research helicopter developed at Universiti Teknologi Malaysia. Figure 1 displays an image of UTM Single-Seat Helicopter which is undergoing extensive research development process. The main purpose of this research is to ascertain the locality of the critical stress, classify and scrutinize the deformation of the chassis under gross loading as well as an intricate discussion on the structural stiffness of the helicopter chassis.

Figure 1 UTM single-seat helicopter

2.0 RESEARCH PROCEDURE

This research endeavored to evaluate the structural stiffness of the chassis through Finite Element Analysis (FEA) using a designated software and substantiate the results by experimental procedure. Initial analysis on the helicopter chassis was done using Femap

with NX Nastran. Femap is an analysis software used to build finite element models of complex engineering problems as a pre-processor [9]. NX Nastran on the other hand acts as a solver to analyze the model and eventually sends back the result for viewing on Femap as post-processor. Figure 2 and Figure 3 elucidate how the process is done by Femap with NX Nastran.

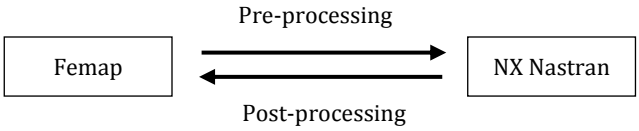

Figure 2 Process flow for Femap with NX Nastran

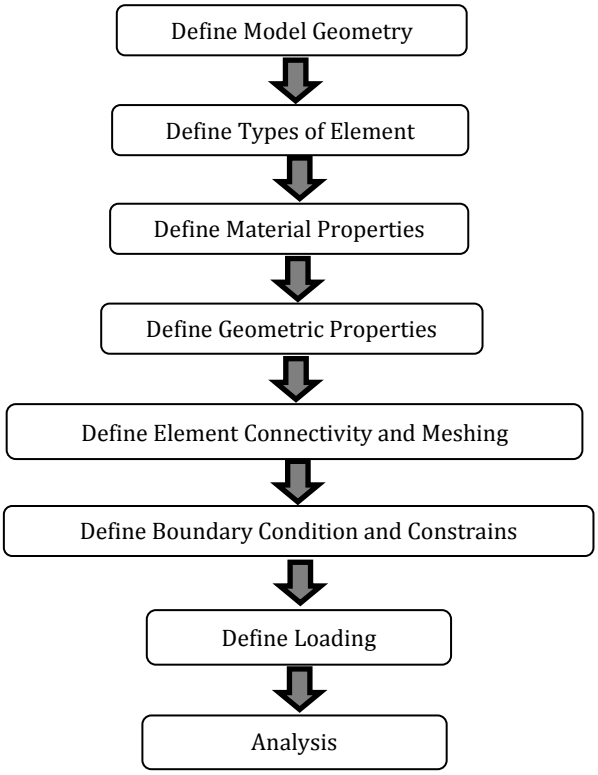

Figure 3 Pre-processing flow of Femap

A specific strain gauge (FLA-6-11) was used in this study. The F series strain gauge is made for general use. The character of '6' in the part number means the gauge length is 6 mm, while '11' is specific code for mild steel. This gauge employs alloy foils between 0.003 to 0.007 mm thick. The back surface of the gauge is made of epoxy resin with thickness of 0.03 mm which exhibits admirable electrical insulation. The back is color coded for distinction of object material and also for self-temperature compensation [10].

Subsequently, National Instrument cDAQ -9172 was used for data acquisition. The main function of this device is to convert the analog signal into digital signal. Basically, analog input generated during the experiment is converted into digital numeric values which is handled by a computer for data reading. However, primarily multimeter was used in this experiment for preparing the experimental setup. It was used to check the connection between the strain gauge and the data acquisition system. Other than that, it was also used to measure the resistant of the lead wire for gauge factor correction. Furthermore, one of the critical points to be discerned was the effects of thermal variation on both the chassis and the strain gauge. Constant measurement of the ambient temperature was taken so that correction can be made due to the apparent strain generated by thermal variation. Ballast was placed at different location on the chassis in order to simulate the loads applied during operation.

3.0 CHASSIS SPECIFICATION

There are different types of chassis which comprises of space frames, monocoque, semi-monocoque etc. Among all these different types of chassis, space frame is often used in motorsport event and high performance vehicles. Space frame chassis is commonly used due to its rigidity and minimalism of construction. Usually in space frames, circular or square tubes are amalgamated together in order to form a lattice structure [5].

UTM Single-Seat Helicopter is constructed using space frame chassis due to its austereness in design and affluence of construction. Usually, for a space frame the load is distributed in axial direction, this ensures that no part of the frame experience severe bending forces [11]. The construction of this helicopter chassis involves the process of welding forty six tubular cylinders to form a lattice structure. There are three types of tubular cylinder with different diameters used to construct the space frame structure. The diameters are 19.1mm, 22.2mm and 12.7mm. Each of them is having the same wall thickness of 1.65mm. Figure 4 demonstrates the helicopter chassis model generated using SolidWorks. Different colors are used for the tubular cylinders in order to identify each type of diameter in the chassis.

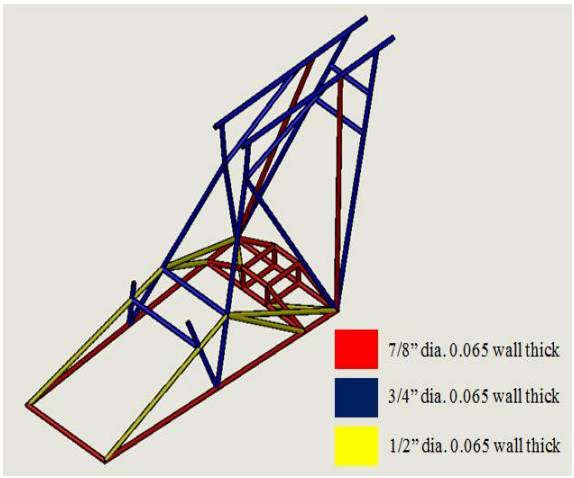

Figure 4 UTM Single-Seat Helicopter chassis

The material used for the chassis construction is AISI 4130 steel. This material can be categorized as high-strength low-alloy (HSLA) steel [12]. This type of steel is commonly used as structural tubing for cars and aircraft frames due to its high strength to weight ratio. Table 1 lists down the AISI 4130 steel properties.

Table 1 Properties of AISI 4130 steel

Properties	Value
Density (kg/m^3)	7850
Ultimate Tensile Strength (MPa)	670
Yield Strength (MPa)	435
Young's Modulus (GPa)	205
Poisson's Ratio	0.29
Hardness (Brinell)	197

4.0 LOADING SPECIFICATION ON THE CHASSIS

This study envisioned to demeanor static analysis on the UTM Single-Seat Helicopter chassis specifically during hovering phase of the helicopter. Five major loads have been identified and considered in the analysis. Table 2 lists all the loads experienced by the helicopter chassis. Figure 5 to Figure 9 illustrate the location and distribution of the loads on the chassis.

Table 2 Loads on chassis

Load	kg	N
Pilot	80	784.80
Engine	50	490.50
Landing Skid	40	392.40
Belting	10	98.10
Tail Boom	25	245.25
Total	**205**	**2013**

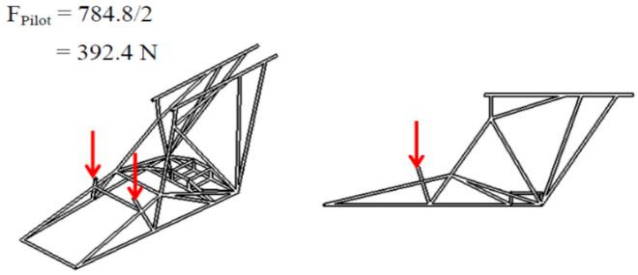

Figure 5 Pilot loading

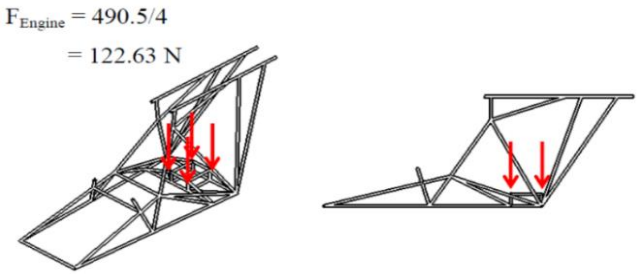

Figure 6 Engine loading

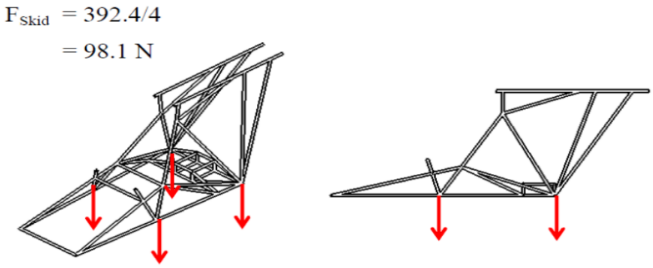

Figure 7 Landing skid loading

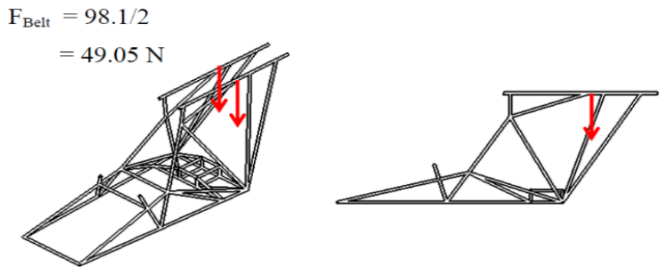

Figure 8 Belting loading

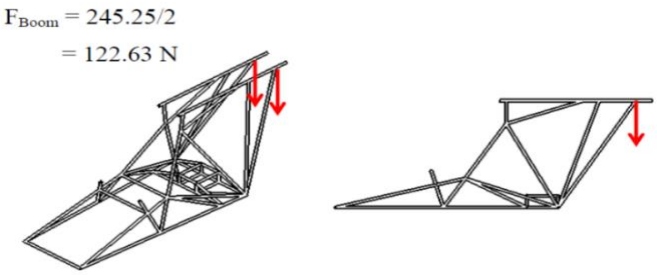

Figure 9 Tail boom loading

In general, anything that is related to civil aviation and aircraft development should comply with certain rules and regulation determined by the authorities. This is to ensure that safety is always considered as the main priority and as a precaution to protect the person on board from undesirable and bewildering incident. Consequently, UTM single-seat helicopter is also designed in compliance with Federal Aviation Regulation (FAR).

UTM Single-Seat Helicopter falls under FAR Part 27 (Normal Category Rotorcraft) as its chassis have a maximum gross load of approximately 700lb (≈ 317.5kg) [13]. Furthermore, the regulation in section 27.303 is concerned on the Safety Factor (S. F). It has been emphasized that S.F must be 1.5 except otherwise declared. This is applicable for both internal and external loads unless internal stresses are easily anticipated.

$$\text{Safety Factor } (S.F) = 1.5$$

$$S.F = \frac{Yield\ stress}{Allowable\ stress} \quad (1)$$

$$S.F = \frac{\sigma_y}{\sigma_{allow}}$$

$$\sigma_{allow} = \frac{\sigma_y}{S.F} \quad (2)$$

$$\sigma_{Allow} = \frac{435\ \text{Mpa}}{1.5}$$

$$\sigma_{Allow} = 290 \text{ MPa}$$

Based on the above calculation, the chassis should be able to support its gross load and also absorb the load generated during the operation while maintaining the minimum safety factor of at least 1.5. The maximum stress σ_{Max}, experienced by the chassis ought to be less than 290 MPa (σ_{Allow}).

■5.0 FINITE ELEMENT ANALYSIS (FEA)

5.1 Creating Geometry

Initially, the structural model of the UTM Single-Seat Helicopter chassis is drawn in Solidworks. The coordinate obtained from Solidworks is then used to create coordinates in Femap (Finite Element Modeling and Post-processing). The geometry is drawn using 'curve-line' command by specifying the coordinate of the point. There are 40 points and 77 curves generated in order to model the chassis. Figure 10 elucidates the curves constructed to model the structural members of the chassis.

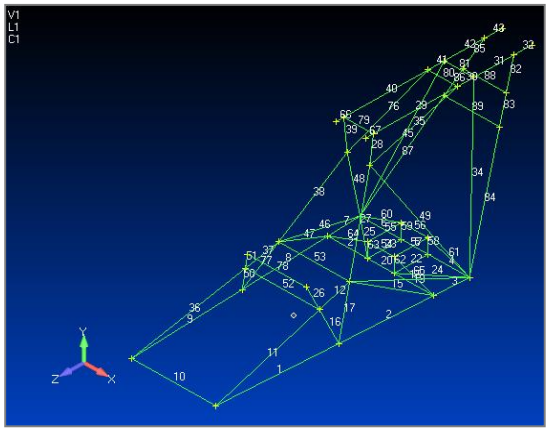

Figure 10 Curves and points generated to model chassis structure

5.2 Meshing Process

The purpose of meshing process is to set the size of elements along the curves. The size of the element is first set to be 1mm for the first iteration of analysis producing 2817 elements and 2780 nodes. The number of elements is later increased by decreasing the size of elements. Table 3 elaborates the model meshing independence study. The value of maximum combine stress and total translation is found to be converging at 39438 elements and 39401 nodes.

Table 3 Meshing independence study

	Elements	Total Translation	Max Stress (Pa)
1	2817	0.00134	35213732
2	5634	0.00134	35214012
3	8451	0.00134	35213040
4	11268	0.00134	35213960
5	16902	0.00134	35216256
6	22536	0.00134	35213792
7	28170	0.00134	35213916
8	39438	0.00134	35218780

The type of element used to model the chassis structure is beam due to its ability to include the effects of transverse shear in the direction of the generated model [14]. Figure 11 shows the meshing process on the chassis model.

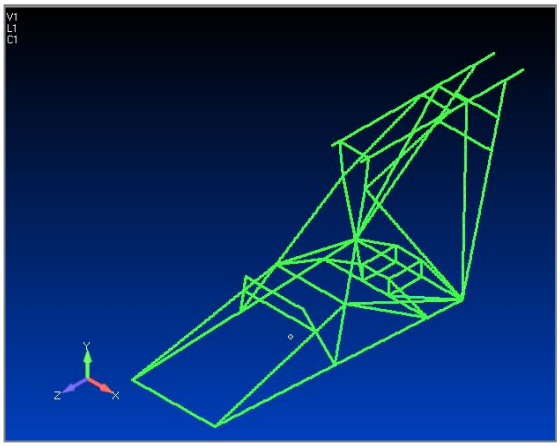

Figure 11 Nodes and elements created by the meshing process

5.3 Material and Geometric Properties

As mentioned earlier, the material used for the chassis structure is AISI 4130 steel. Important properties that requires to be defined for the analysis are Young's Modulus, E = 205 GPa; Poisson's Ratio, v = 0.29 and density, ρ = 7850 kg/m^3. The chassis is made of tubular cylinder with three different sizes of diameter where each of them is having the same wall thickness. Figure 12 shows the model after the application of material and geometric properties.

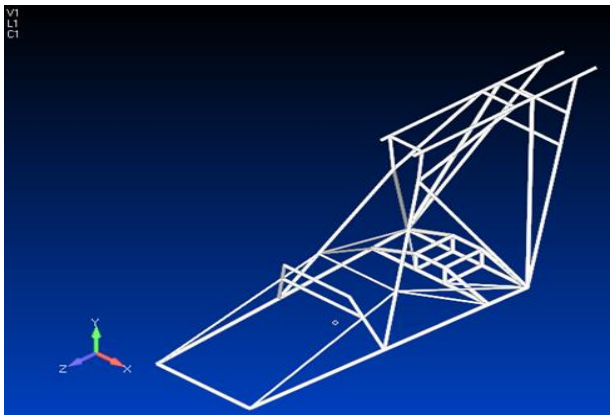

Figure 12 Chassis model upon the application of material and geometric properties

5.4 Boundary Condition

During hovering phase, the load is fully exerted on the chassis. At this juncture, constrain was applied on the location where the chassis is attached to the helicopter main shaft mounting point. Furthermore, the chassis is set to be fixed in all direction, which implies that there is no translation and rotational motions. Figure 13 shows the boundary condition during hovering condition.

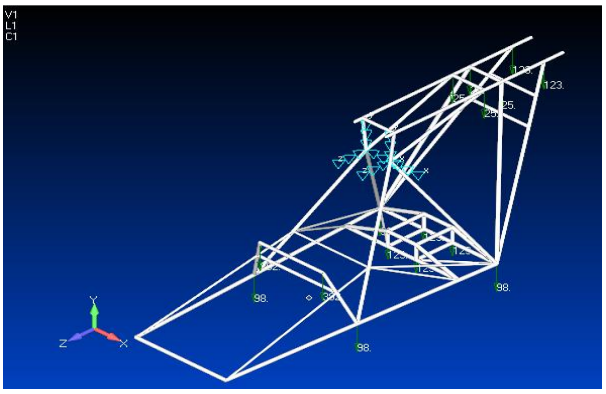

Figure 13 Hovering phase boundary condition

■6.0 EXPERIMENTAL SETUP AND PROCEDURE

The output result from the experiment is used to compute the strain and stress occurring on the chassis. Then the experimental data is compared with the results obtained from finite element simulation. Figure 14 illustrates how the static strain test is conducted on the helicopter chassis.

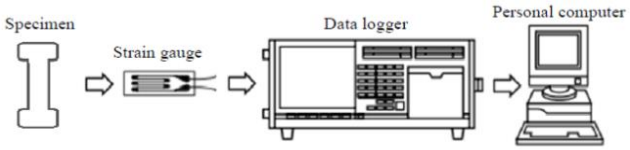

Figure 14 General setup for static strain test

Initially, attaching the strain gauge on the helicopter chassis is the most crucial process in preparing the experimental setup. Strain gauge requires to be properly mounted on the specimen so that the strain experienced by the specimen test will directly transfer to the strain gauge. Usually, corrupt specimen contribute towards error and eventually produce unacceptable result. Figure 15 shows the location determined on the chassis where the strain gauge is to be attached. The specified area is sanded slightly larger than the bonding area uniformly and finely with abrasive papers. The bonding area was cleaned with tissues soaked in a small quantity of acetone. Then, the cleaning was done until the area is completely free from any contaminations. Certain amount of adhesive was dropped onto the back of the gauge surface. Then, the adhesive was spread over the surface thinly and uniformly. Polyethylene sheet was used to place the gauge on the specified area as shown in Figure 16. After that, the gauge was pressed down constantly for approximately 60 seconds.

Subsequently, the strain gauge lead wire is attached to the data logger and they are marked individually to avoid any sorts of confusion of the channels. Initially, the helicopter is sitting on the ground and the total weight of the helicopter is fully supported by the landing skid. Just before the experiment initiated, the reading of the ambient temperature is taken along with the zero strained data. Figure 17 shows how the load is applied on the helicopter chassis. Afterwards, the helicopter is lifted up approximately 10 centimeters (cm) from the ground where the landing skid is not touching the ground and the load is fully supported at main shaft mounting point as shown in Figure 18. Then the strained reading is taken and this same process is reiterated three times.

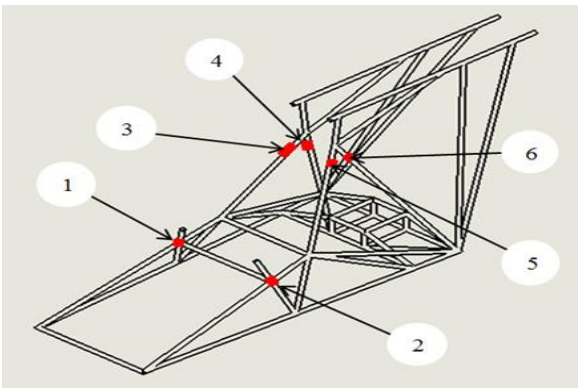

Figure 15 Location of strain gauge on the chassis

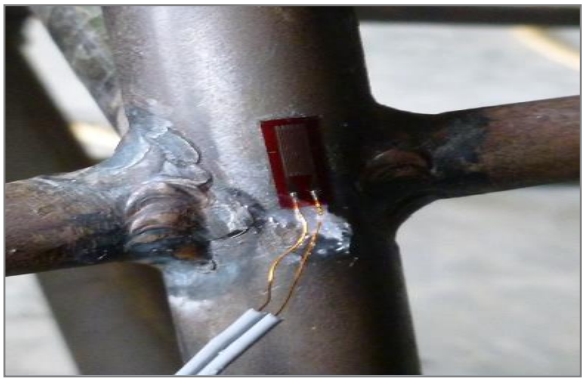

Figure 16 Strain gauge mounted on the chassis

Figure 17 Loads on the chassis

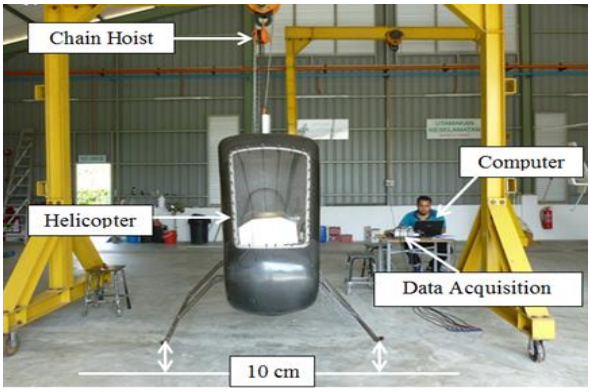

Figure 18 Experiment setup

7.0 RESULTS AND DISCUSSION

7.1 Maximum Stress

Figure 19 demonstrates the maximum combined stress distribution on the chassis. The maximum stress transpires to be 35.22 MPa. It is clearly evident that the maximum stress occurs at structural joint of the pilot seat. According to the initial calculations, it was anticipated earlier that the pilot was the heaviest load acting on the chassis. Figure 20 shows the joint on the pilot seat where maximum stresses is occurring.

Large span of the structural member on the pilot seat contribute towards the generation of highest stress at the joints. Henceforth, this part is taken into critical contemplation. Extra tubes in traverse direction might substantially be considered for additional support if necessary. Figure 21 depicts original and deformed model of the helicopter chassis due to maximum combined stress.

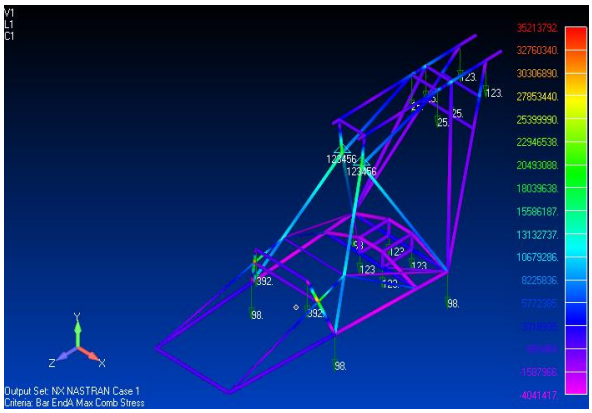

Figure 19 Maximum combined stress distribution

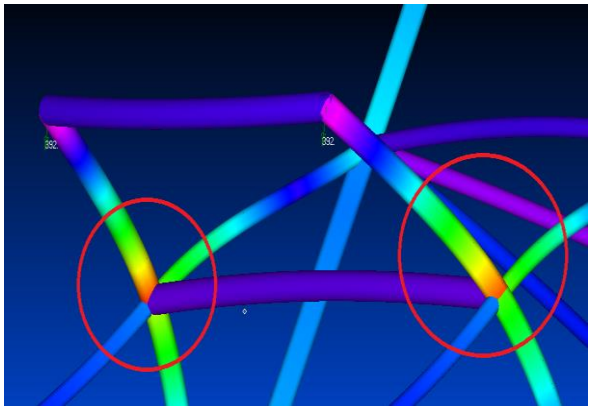

Figure 20 Location of maximum stress on the chassis

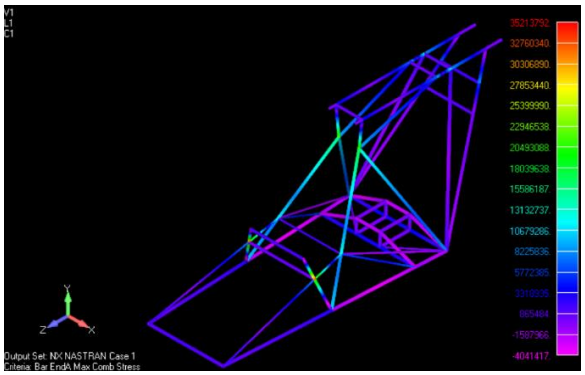

(a) Undeformed Model

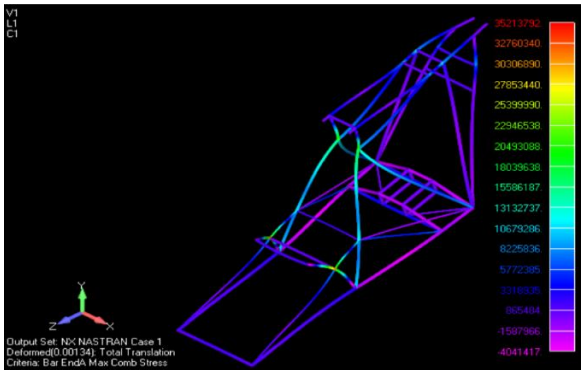

(b) Deformed Model

Figure 21 Maximum combined stress

7.2 Deformation

Figure 22 displays the total translation of the chassis. The maximum displacement is 1.34 mm and located at the front section of the helicopter chassis. As predicted, this occurs where the pilot's load is acting. The load from pilot contribute towards deformation dispersal and eventually causing the maximum deformation to occur at the front section of the chassis. Figure 22 demonstrates the original and maximum deformation of the UTM Single-Seat Helicopter chassis.

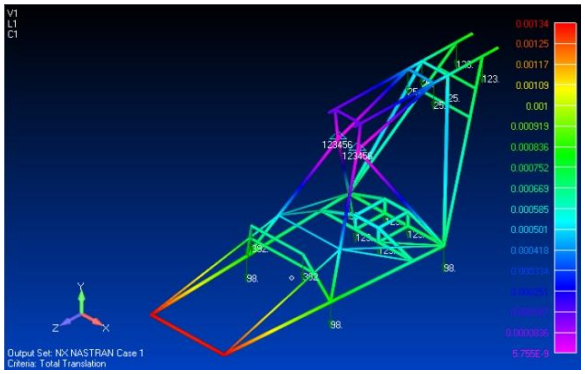

Figure 22 Deformation on the chassis

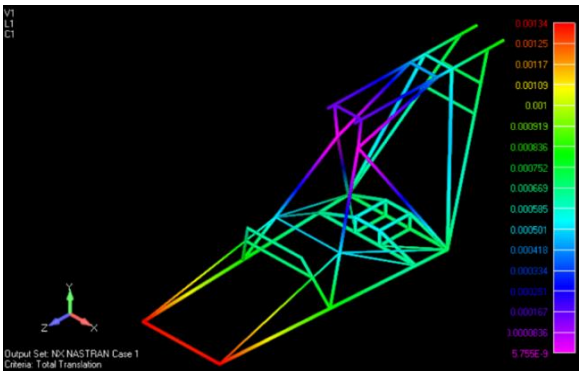

(a) Undeformed model

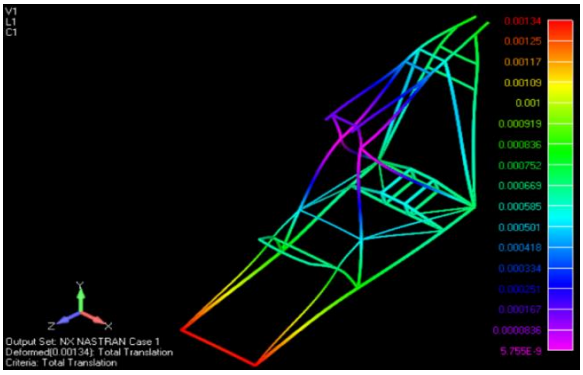

(b) Deformed model

Figure 23 Maximum deformation

7.3 Chassis Strength

Based on the results, UTM Single-Seat Helicopter chassis is found to be capable of supporting the gross load during hovering condition because the maximum stress (σ_{max}) experienced by the chassis is well below the material yield stress. The safety factor of the chassis during hovering condition is 13.23 which is greater than 1.5. Consequently, this implies that the chassis acts in accordance with the terms of FAR Part 27, section 27.303.

$$\sigma_{max} < \sigma_y$$

$$32.87 \text{ Mpa} < 435\ Mpa$$

$$S.F = \frac{\sigma_y}{\sigma_{max}}$$

$$S.F = \frac{435.00}{32.87} = 13.23$$

7.4 Result Comparison

Comparison of the results is conducted in order to verify both the experimental and analytical data. There are six locations for the installed strain gauges. Each location is different from one another. Table 4 demonstrates the difference between FEA simulation and experiment. The results show that the maximum stress for both experiment and FEA simulation have practically the same predilection. Experiment results have efficaciously substantiated that the location of the maximum stress occurring on the chassis is at the pilot's seat pillar. The maximum stress experienced by the chassis is 32.87 MPa located at strain gauge number '2'. Result difference at each point is smaller than 10 percent, with the maximum difference occurring at strain gauge number '5' which is 9.7 percent. The minimum error occurs at strain gauge number '3' with 5.09 percent.

Table 4 Comparison between experiment and FEA

Strain Gauge Number	Maximum Stress, Mpa		Difference %
	Experiment	FEA	
1	32.40	35.21	8.01
2	32.87	35.21	6.65
3	17.45	16.61	5.09
4	13.09	12.16	7.59
5	18.22	16.61	9.70
6	13.09	12.16	7.59

7.5 Factors Contributing to the Result Variation

There are perceptible differences between the results obtained from the experiment and FEA simulation. The two main factors contributing towards the result variation are temperature and the inconsistency of fabrication. They are discussed further in the following section.

7.5.1 Variation of Temperature

In the process of conducting static strain test on a specimen, the only desirable strain is the strain generated due to the applied loads. Ill-advisedly the specimen and the gauge material is also be exposed to the environment which indirectly responds to the thermal discrepancy. In other words, the specimen and the strain gauges experience apparent strain prior to the application of the loads. Initially during the experiment, the ambient temperature for the first reading have been found to be 33°C. The temperature continuously changed for the second and the third attempt with the ambient temperature of 30.5°C and 28°C respectively. The strain gauge resistance varies due to vicissitudes of the ambient temperature. For greater accuracy, corrections can be made using the curves for apparent strain against temperature portrayed in Figure 24, this is usually supplied with each package of stain gauge. However, it is to be noted that the compensated gauge only aids in reducing the thermal sensitivity but do not entirely remove the apparent strain.

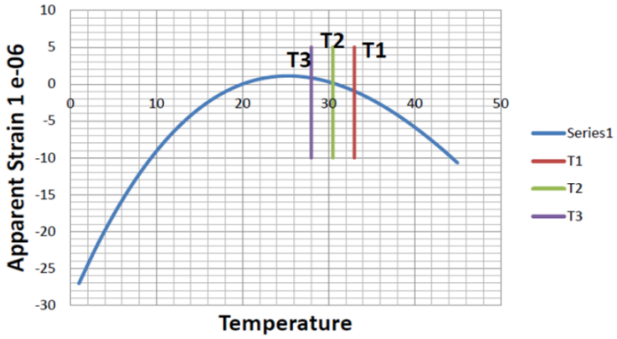

Figure 24 Apparent strain due to thermal sensitivity

7.5.2 Fabrication Discrepancy

Another major factor that contributes to the result variance is the inconsistency of fabrication on the chassis. It is exceedingly challenging to make sure that the chassis is having the precise dimensional exactitude since it is neither welded by a machine, nor casted in a mold. Each section is individually manufactured and assembled. Figure 25 illustrates some of the irregularities during fabricating process of the chassis. Consecutively, during FEA design and analysis process, the chassis is assumed to be smooth (i.e. ideally welded) with every contact point at each joint, while in real occasion, there are several contact points at each joint on the chassis. This factor affects the load distribution on the chassis which eventually cause the result discrepancy between experiment and FEA simulation.

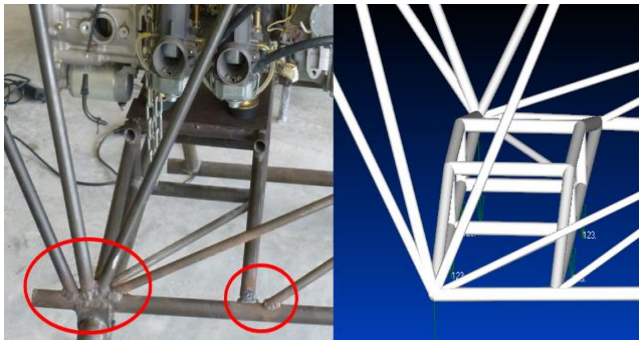

Figure 25 Inconsistency of fabricating on the chassis

8.0 CONCLUSION

The main object of this study was to determine the location of critical point which has the highest stress for the UTM Single-Seat Helicopter chassis. The study was carried out using Finite Element Analysis simulation and experimental test. Although, there are factors such as variation in temperature and inconsistency of fabrication contribute to the result disparity, the results obtained found that the inclination for maximum stress was virtually similar for both experiment and FEA simulation. Consequently the result obtained by FEA simulation was corroborated by the experiment experimental results. Additionally, the maximum stress occurring on the chassis is 32.87 MPa at pilot seat pillar and the maximum deformation is 1.34 mm located at the front section of the chassis. This chassis is able to support the loading condition set in this study and comply with FAR Part 27 as the maximum stress is well below the material yield stress. Nevertheless, extensive and arduous research is being done continuously on the UTM Single-Seat Helicopter to improve its performance. Buoyantly, it may become one of the significant landmarks in applied engineering for Malaysia in the near future.

Acknowledgement

The authors would like to thank Universiti Teknologi Malaysia for providing valuable support to conduct this research project. Vot. Number Q.J130000.2424.00G66.

References

[1] Z.B.A. Awal, M. S.B. Ammoo. 2014. *A Case Study on the Air Flow Characteristics of the Hirobo-FALCON 505 Controllable Helicopter's Main Rotor Blade*. Applied Mechanics and Materials. 527: 39–42.

[2] M.S.B. Ammoo, Z.B.A. Awal. 2013. *Main Rotor Blade Air Flow Characteristics & Behaviour of a Remote Controlled Sub-scale Helicopter: A Case Study*, International Journal of Research in Aeronautical and Mechanical Engineering. 1(7): 228–235.

[3] Z.B.A. Awal, M.S.B. Ammoo, N.S.B. Jamaluddin. 2014. *The Effect of Rotor Disc Clearance on the Lift Performance of Contra-Rotating Rotor Blades*. International Journal of Research in Engineering and Technology. 3(5): 739–745.

[4] M.S.B. Ammoo, Z.B.A. Awal. 2014. *An Investigation on Crack Alleviation in Bending of Aluminium 2024 for Aircraft Application*. International Journal of Research in Aeronautical and Mechanical Engineering. 2(3): 255–269.

[5] M.H.Mat, A.R.A. Ghani. 2012. *Design and Analysis of 'Eco' Car Chassis*. Procedia Engineering. 41: 1756–1760.

[6] T. Limwathanagura, C. Sithananun, T. Limchamroon, T. Singhanart. 2012. *The Frame Analysis and Testing for Student Formula*. World Academy of Science, Engineering and Technology. 6: 1058–1062.

[7] M.S.F.B. Hashim. 2008. *Design and Analysis of a 2-seater Helicopter Fuselage Structure*. Final Year Undergraduate Project Thesis. Faculty of Mechanical Engineering, Universiti Teknologi Malaysia.

[8] M.A.M. Nor, H. Rashid, W.M.F. W. Mahyuddin, M.A.M. Azlan, J. Mahmud. 2012. *Stress Analysis of a Low Loader Chassis*. Procedia Engineering. 41: 995–1001.

[9] T.R. Chandrupatla, A.D. Belegundu. 2002. *Introduction to Finite Elements in Engineering*. Prentice Hall. 3rd Edition.

[10] TML Pam-E101S. 2012. TML Strain Gauge Catalog. (Web link: https://www.tml.jp/e/download/catalog/ProductGuide_E950Q.pdf)

[11] K.J. Wakeham. *Introduction to Chassis Design*. 2009. University of Newfoundland and Labrador. 1st Edition. (Web link: http://www.keithwakeham.com/Files/ChassisDesign.pdf)

[12] W.D. Callister. 2007. *Material Science and Engineering: An Introduction*. 7th Edition.

[13] Normal Category Rotorcraft. *Federal Aviation Regulation*. FAR Part 27. (Web Link: http://www.risingup.com/fars/info/27-index.shtml)

[14] R.P. Singh. 2010. Structural Performance Analysis of Formula SAE Car. Chitkara Institute of Engineering and Technology. *Jurnal Mekanikal*. 31: 46–61